ISTITUTO NAZIONALE DI FISICA NUCLEARE

Sezione di Genova

INFN/AE-84/7
23 Luglio 1984

A. Buzzo, M.G. Pia and A. Santroni:

A DETECTOR TO STUDY ξ(2220) AT LEAR

Servizio Documentazione
dei Laboratori Nazionali di Frascati

INFN - Istituto Nazionale di Fisica Nucleare
Sezione di Genova

INFN/AE-84/7
23 Luglio 1984

A DETECTOR TO STUDY $\xi(2220)$ AT LEAR

A. Buzzo, M.G. Pia and A. Santroni
INFN - Sezione di Genova, (Italy) and Dipartimento di Fisica dell'Università di Genova, (Italy).

1. - INTRODUCTION

The technique of having an accumulated antiproton beam traversing a hydrogen jet target was recently used successfully at the ISR in the experiment R704 to study charmonium states[1].

In March 1984 a letter of intent[2] was sent to the CERN Committee to propose to install the Hydrogen Jet Target in LEAR to study the formation of small width resonant states in $p\bar{p}$ annihilation.

As a contribution to this we have considered in this paper the possibility of a 'first generation' experiment at LEAR before the ACOL shutdown. Due to the short time available, the following practical limitations were taken into account:

1) no modification to the jet target, including the R704 vacuum chamber, is possible;
2) the experimental apparatus should be as simple as possible and should use most of the R704 detectors and electronics.

As to the physics, the study of the recently discovered $\xi(2220)$ state was considered, whose K^+K^- and $K^o_s K^o_s$ decays were detected by the MARK III experiment at SLAC[3] and $\phi\phi$ decay is in principle possible.

The reaction

$$p\bar{p} \rightarrow \xi \rightarrow \phi\phi \rightarrow K^+K^-K^+K^- \qquad (1)$$

was studied with a Montecarlo simulation. Preliminary indications are also given for the reactions

$$p\bar{p} \rightarrow \xi \rightarrow K^o_s K^o_s \rightarrow \pi^+\pi^-\pi^+\pi^- \qquad (2)$$

and

$$p\bar{p} \rightarrow \xi \rightarrow K^+K^- \qquad (3)$$

The ξ mass is assumed to be 2.22 GeV; the corresponding antiproton beam momentum is 1.403 GeV/c.

Event generation is isotropic in centre of mass; the vertex is generated inside an interaction region of 1 cm^3.

The kinematical features of reaction (1) are shown in Fig. 1; on this basis the acceptance of some detector configurations is studied (Chapter 2.).

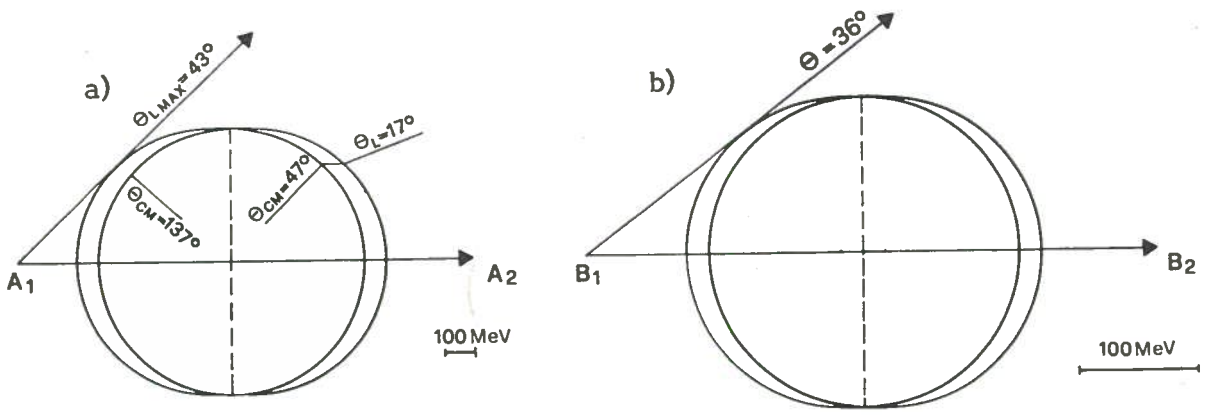

FIG. 1 - a) $p\bar{p} \rightarrow \xi \rightarrow \phi\phi$ kinematics (A1-A2 is the antiproton beam momentum); b) $\overline{\phi \rightarrow K^+K^-}$ kinematics (p(ϕ) = 450 MeV/c) (B1-B2 is the ϕ momentum).

A possible method of particle identification is discussed in Chapter 3. together with some preliminary studies of background processes.

The characteristics of a detector system suggested by the Montecarlo simulation are described in Chapter 4.

2. - ACCEPTANCE

The study of the acceptance was essentially related to the detection of the reaction

$$p\bar{p} \rightarrow \xi \rightarrow \phi\phi \rightarrow K^+K^-K^+K^- \qquad (4)$$

Results are also given for the processes

$$p\bar{p} \rightarrow \xi \rightarrow K^0_S K^0_S \rightarrow \pi^+\pi^-\pi^+\pi^- \qquad (5)$$

$$p\bar{p} \rightarrow \xi \rightarrow K^+K^- \qquad (6)$$

assuming an apparatus configuration optimized for reaction (4).

2.1. - Angular Acceptance

The acceptance was studied for different configurations of the apparatus. Events with the directions of all the 4 K inside the angular limits of the apparatus were accepted.

The acceptance values resulting from high statistics runs (20000 events) are listed in Table I.

The configuration 4), corresponding to a 4-arm apparatus, with parameters as in Table II, was

TABLE I - Angular acceptance for some configurations.

The apparatus configurations, all with $17° < \theta < 66°$, correspond to:

1. 2 arms, $\Delta\varphi = 90°$ each.
2. 4 arms, $\Delta\varphi = 45°$ each, centred $\varphi = 0°, 90°, 180°, 270°$;
3. 4 arms, $\Delta\varphi = 45°$ each, centred $\varphi = 45°, 135°, 225°, 315°$;
4. 2 pairs of arms, centred $\varphi = 0°, 180°$, 10° separation;
5. 2 pairs or arms, centred $\varphi = 0°, 180°$, 5° separation;
6. 2 pairs or arms, centred $\varphi = 45°, 225°$, 10° separation;
7. 2 pairs of arms, centred $\varphi = 0°, 180°$, 20° separation;
8. 2 pairs or arms, centred $\varphi = 0°, 180°$, 30° separation.

Configuration	Acceptance
1	7.54
2	2.18
3	2.16
4	6.03
5	6.90
6	6.53
7	4.15
8	2.56

TABLE II - Basic angular configuration.

ARM	THETA (degrees)	PHI (degrees)
1	17 - 66	-50 - -5
2	17 - 66	5 - 50
3	17 - 66	130 - 175
4	17 - 66	-175 - -130

chosen as the most practical, since it is possible to use some detectors of the existing R704 apparatus (small MWPC's). All the following results were calculated assuming this configuration.

The momentum spectrum of the K inside the angular acceptance thus defined is plotted in Fig. 2.

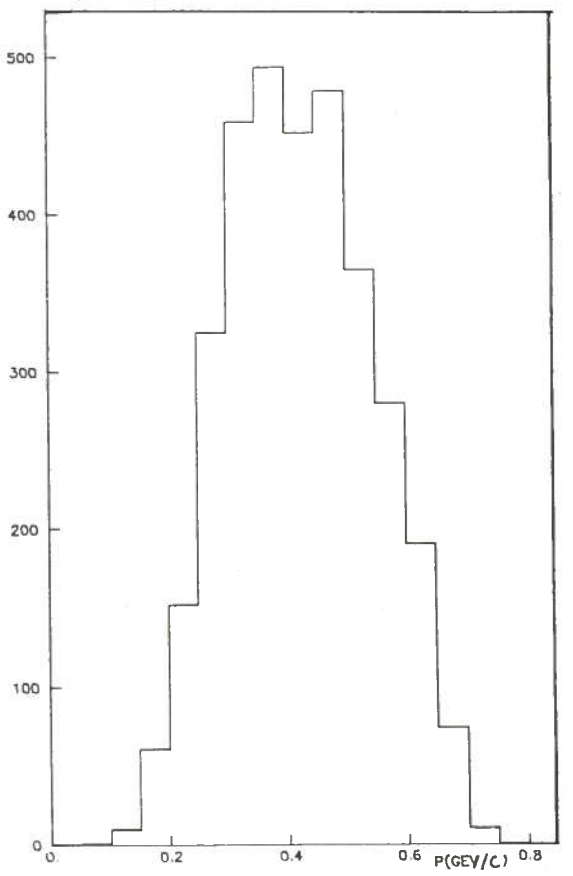

FIG. 2 - Momentum spectrum of accepted K from $\emptyset\,\emptyset$.

2.2. - K Decay

K decay was simulated according to the distribution

$$dN(t) = N(0) \exp(-t/t_o)\, dt$$

where t_o is the particle lifetime.

The distribution of the Z-coordinate of the K decay point is shown in Fig. 3.

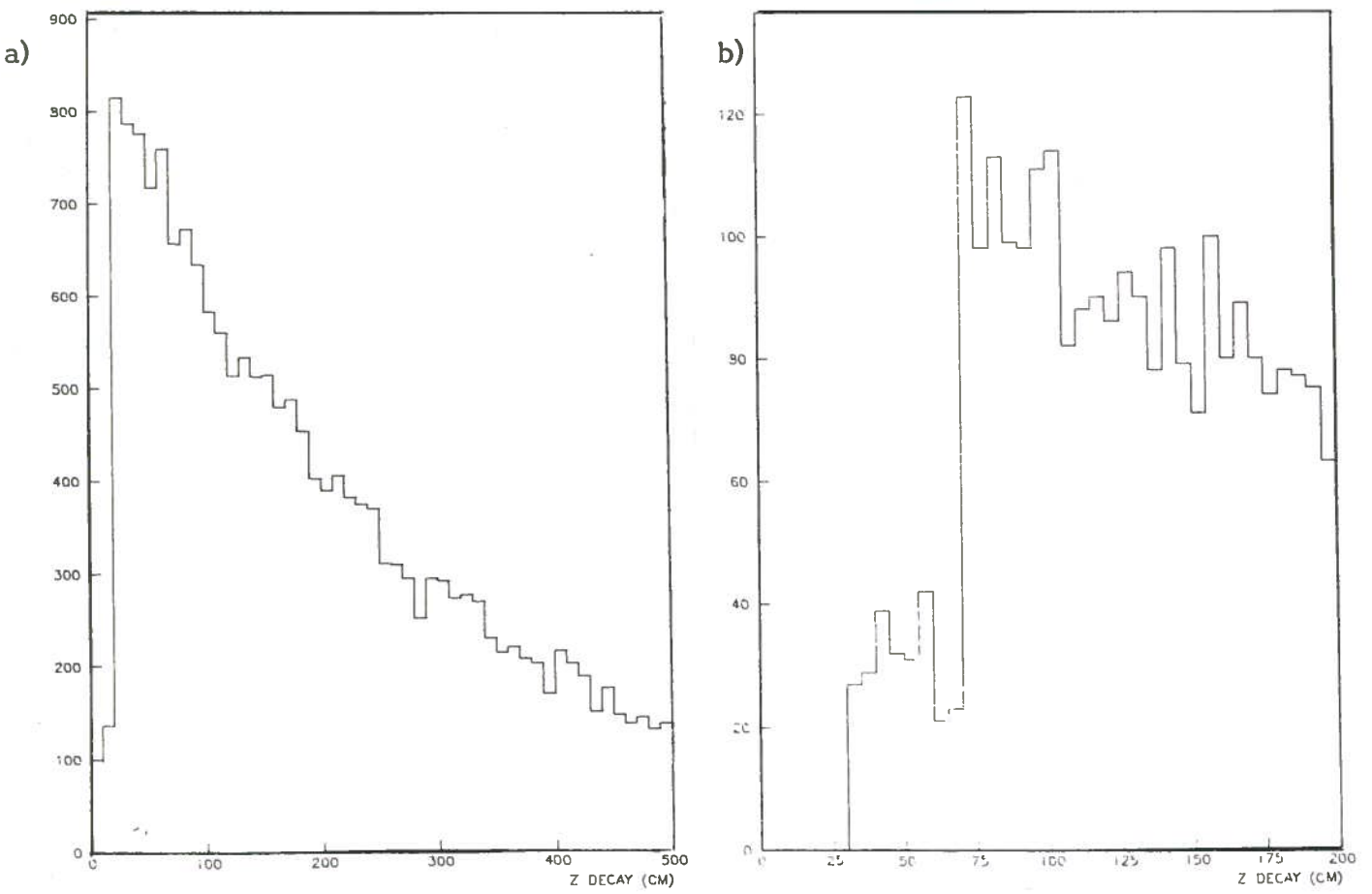

FIG. 3 - a) Z local distribution for K decay; b) Z local distribution for K decaying after CH1.

K decay reduces the acceptance very much: the acceptance for some values of the upper Z-limit Zmax of the apparatus, requesting that 4 K decay after Zmax, is shown in Table III.

TABLE III - Acceptance versus Zmax (local coordinate along arm axis).

ZMAX (cm)	ACC.(%)
50	2.86
60	2.83
70	2.19
100	1.40
120	1.06

As a consequence of this effect the experimental apparatus should be as compact as possible; a lowest limit for Zmax was assumed in the Montecarlo calculation as Zmax=70 cm.

For this value of Zmax the possibility of requesting 3 K in the apparatus at least was considered; in this case the kinematics of the event would be determined all the same, even if without any constraint. With this request the acceptance is =11% for Zmax=70 cm.

2.3. - Multiple Scattering

Multiple scattering in the vacuum chamber sail was simulated with a gaussian distribution according to the formula

$$\theta_{RMS} = 0.021/(p\beta)\sqrt{X/x_o}\,(1+0.1)$$

where x is the path traversed and x_o=1.77 cm is the iron radiation length.

The configuration of the vacuum chamber was assumed as in Fig. 4a, with a 0.3 mm iron thickness; a fine approximation of the profile was simulated.

The distribution of multiple scattering angle is plotted in Fig. 4. This resulted also in a small decreasing in the acceptance, as it is shown in Table IV.

2.4. - Basic Configuration Acceptance

A standard set-up was assumed, corresponding to configuration 4) as in Table II and in Fig. 5, with Zmax=70 cm. In this simulation, including the effect of multiple scattering, the event rejection can be summarized as follows:

1) requesting 4 K inside the acceptance:
   - 4.1.% of the events pass the angular cuts;
   - 1.9% of the events pass also the Zmax cut;
2) requesting 3 K at least inside the acceptance:
   - 15.1% of the events pass the angular cuts;
   - 9.7% of the events pass also the Zmax cut.

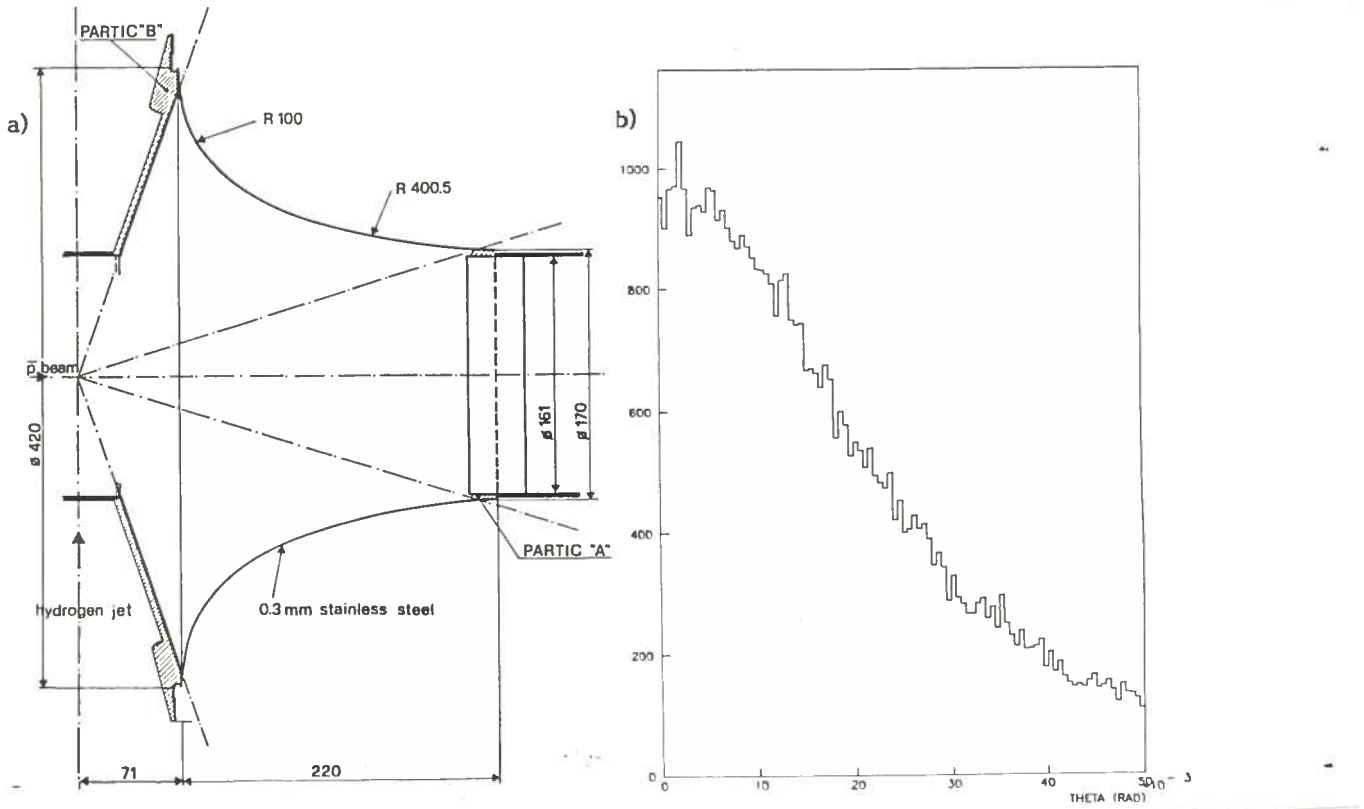

FIG. 4 - a) Vacuum chamber longitudinal section; b) Distribution of K multiple scattering angle through the vacuum chamber.

TABLE IV - Effect of multiple scattering on the acceptance.

Request	Without mult.sc.	With mult. sc.
⩾ 3 K	10.9 %	9.7 %
4 K	2.2 %	1.9 %

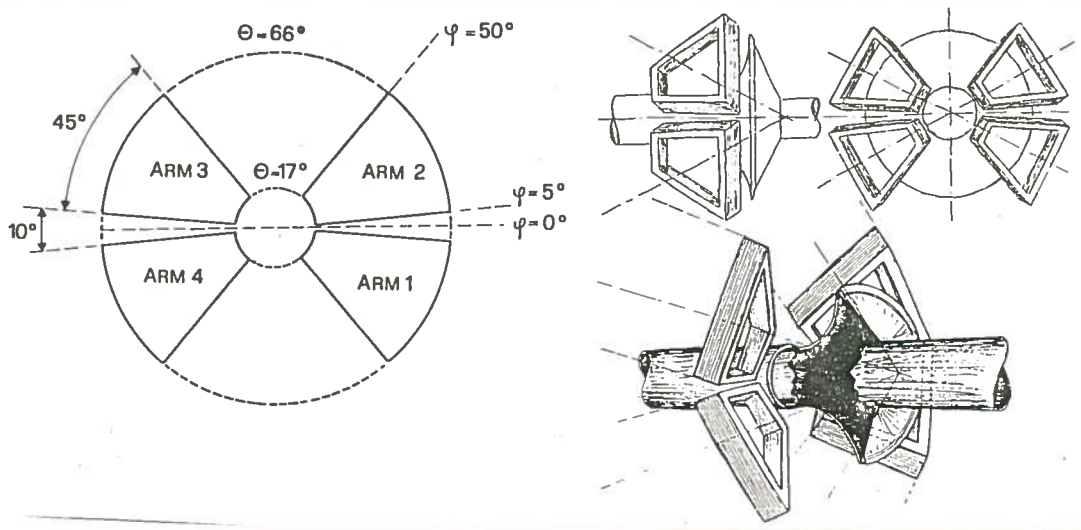

FIG. 5 - a) Angular limits for the basic configuration; b) Sketch of a 4-arm system (only CH1 at Z-local = 35 cm is shown).

All the following results were obtained assuming this configuration of the apparatus and requesting 3 K at least in the acceptance.

The 4th K can be outside the angular acceptance or can decay before Zmax; in this case, if it decays inside the apparatus, it can be recuperated. Therefore the real acceptance will be between 2% and 10%.

The angular distribution and the Z-coordinate of the decay point of the fourth K escaping detection are shown in Figs. 6b and 6c.

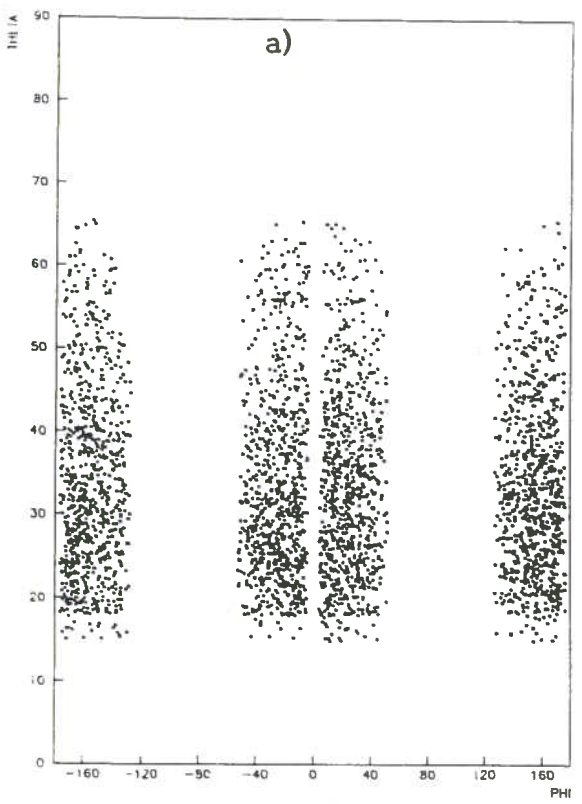

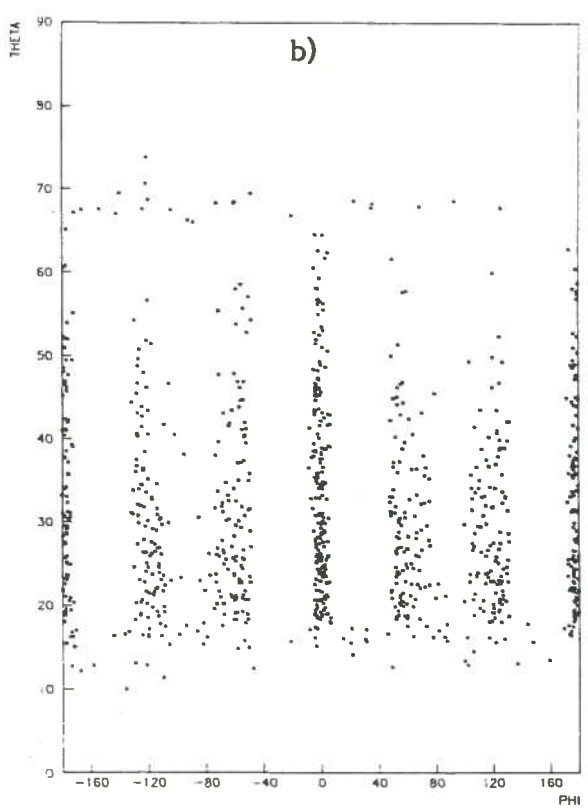

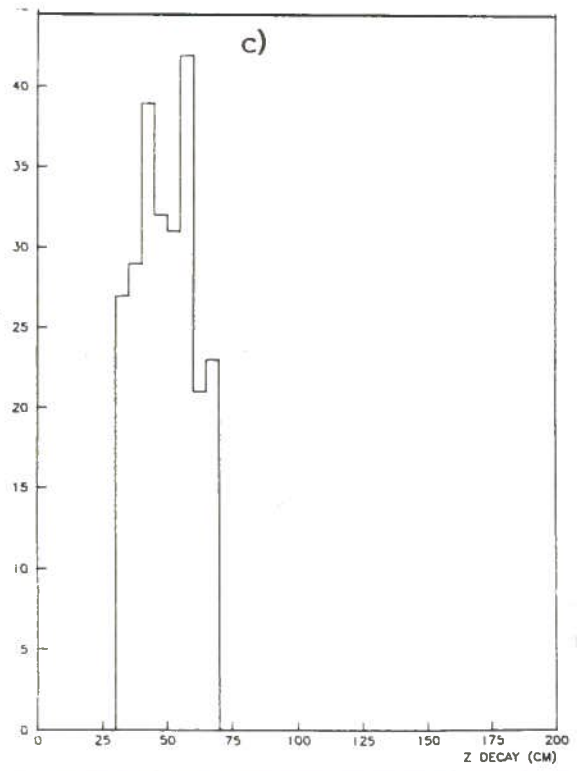

FIG. 6 - a) (θ, ϕ) for the accepted K, b) (θ, ϕ) of the fourth K outside the angular acceptance, the other three K being inside, c) Distribution of Z-decay coordinate for K decaying inside the apparatus.

2.5. - Acceptance for other Processes

The acceptance was calculated also for the processes

$$p\bar{p} \rightarrow \xi \rightarrow k_s^o K_s^o \rightarrow \pi^+\pi^-\pi^+\pi^- \quad (7)$$

$$p\bar{p} \rightarrow \xi \rightarrow K^+K^- \quad (8)$$

assuming the standard set-up described in Sect. 2.4. The following values were obtained:

a) reaction (7):

- 0.37% requesting 4π inside the acceptance;
- 6.7% requesting 3π at least inside the acceptance.

b) reaction (8):

- 9.98% requesting both the K inside the acceptance.

3. - PARTICLE IDENTIFICATION

As a possible method of particle identification, energy loss-range correlation was studied. The momentum spectra of the accepted final state particles of

$$p\bar{p} \rightarrow \xi \rightarrow \phi\phi \rightarrow K^+K^-K^+K^- \quad (9)$$

$$p\bar{p} \rightarrow \xi \rightarrow k_s^o K_s^o \rightarrow \pi^+\pi^-\pi^+\pi^- \quad (10)$$

$$p\bar{p} \rightarrow \xi \rightarrow K^+K^- \quad (11)$$

are plotted in Fig. 7. The identification method proposed is practicable in the region of low momenta ($<$700 MeV/c); so it can be applied with a significant efficiency to reaction (9) only, while it can only partially help in rejecting some background events in the other cases.

The following discussion concerns reaction (9); preliminary considerations for the other processes are given in Sect. 3.5.

A set of analog chambers[1] and a sandwich of Pb layers and active planes were considered as detectors performing particle identification.

3.1. - Energy Loss Measurement

The mean energy loss in analog chamber gaps was computed according to the Bethe-Salpeter formula, with some approximations valid in this energy range:

$$dE/dx = a/\beta^2 \log(4\, b\beta\gamma)$$

where a and b are constants depending on the medium. Analog chambers were assumed to be filled with pure Argon.

Landau fluctuations around the most probable energy loss were taken into account; they were generated according to the following formula, resulting from a fit to experimental data[4]:

$$f(\lambda) = a1 * \exp\{-a2(\lambda + a5 * \lambda^2) - a3 * \exp(-a4(\lambda + a6 * \lambda^2))\}$$

where: $\lambda = (eloss - eloss_{mp})/x + \lambda_{mp}$; x depends on the medium, on the length traversed and on β.

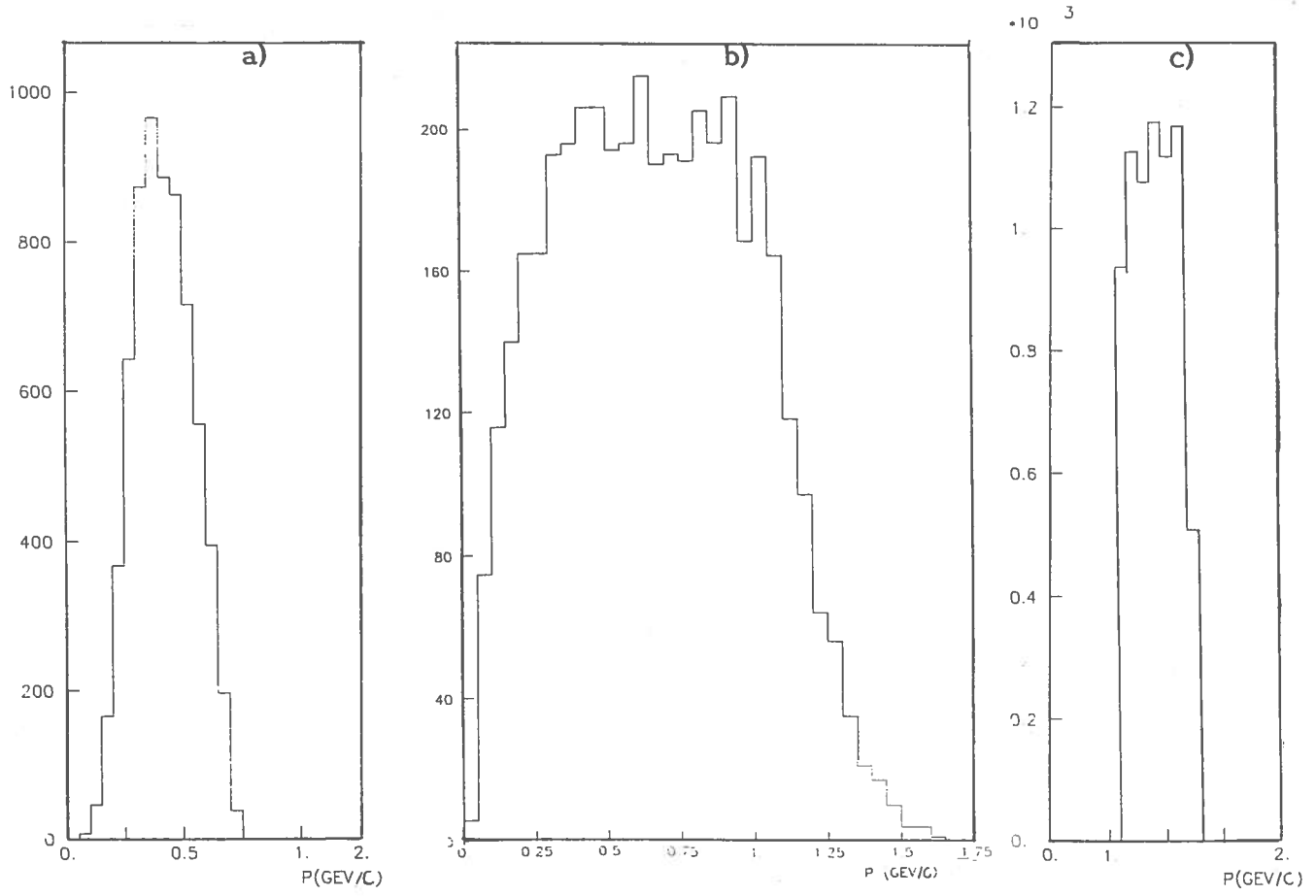

FIG. 7 - Momentum spectra in the acceptance for: a) 4 K from $\phi\phi$, b) 4π from $K_s^o K_s^o$, c) $K^+ K^-$ from ξ.

The Landau distribution thus generated for a 1 cm gap of Ar is plotted in Fig. 8 for the K in the accepted spectrum.

A set of independent energy loss samplings was simulated to reduce the uncertainty in the energy loss measurement due to Landau fluctuations; to this purpose the method of "truncated mean" was used to extract the information: the mean energy loss was calculated as the average of the N lowest values out of NTOT measurements. The performance of this method in cutting the tails of the Landau distribution is shown in Figs. 9 and 10, where the energy loss is plotted as a function of β. The effect of the choice of different numbers of analog chamber planes and of the corresponding fraction of mesurements to retain is shown in Fig. 11.

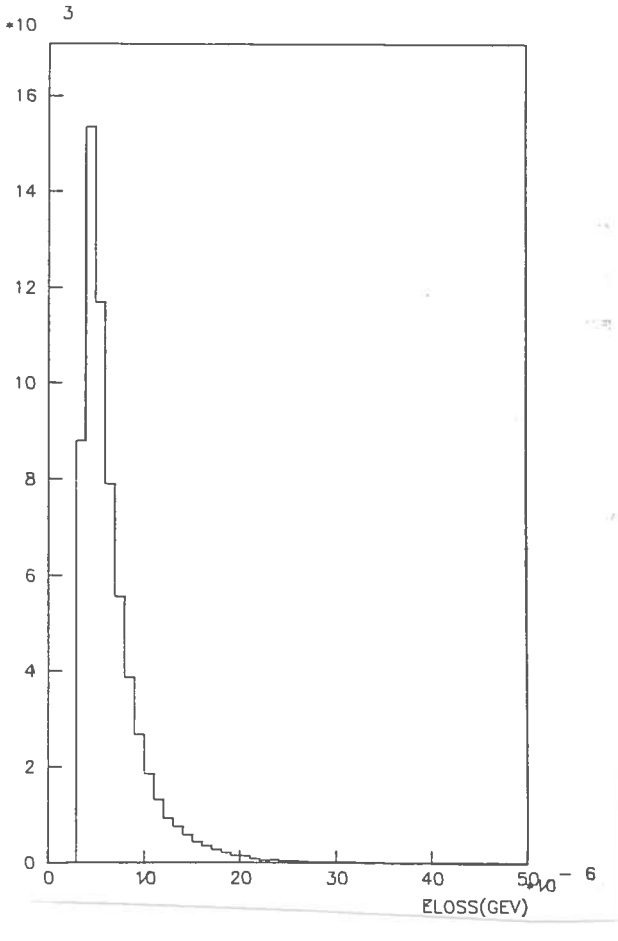

FIG. 8 - Energy loss in 1 cm Argon (NTP) for the accepted K momenta.

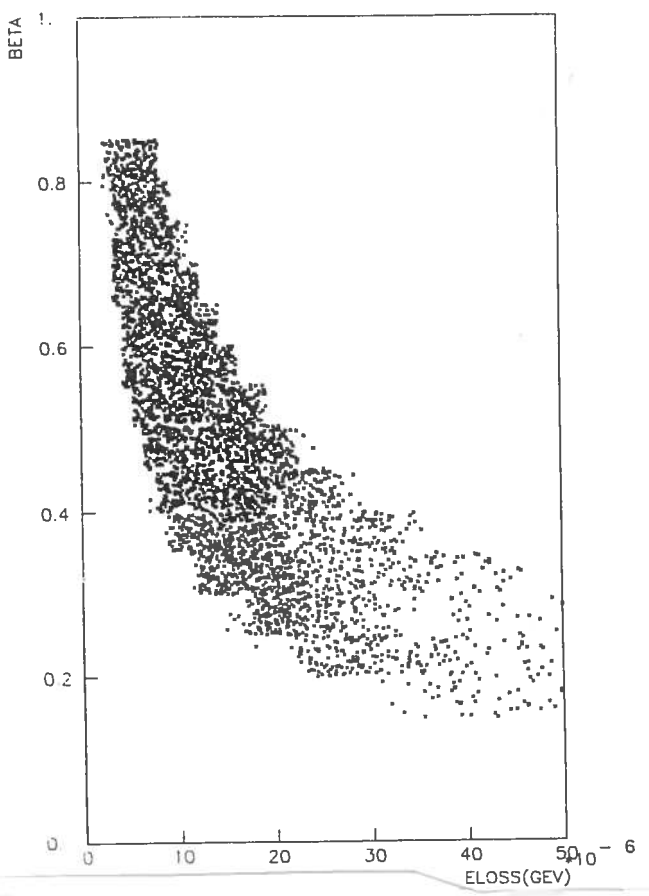

FIG. 9 - β versus energy loss, 1 cm Ar gap.

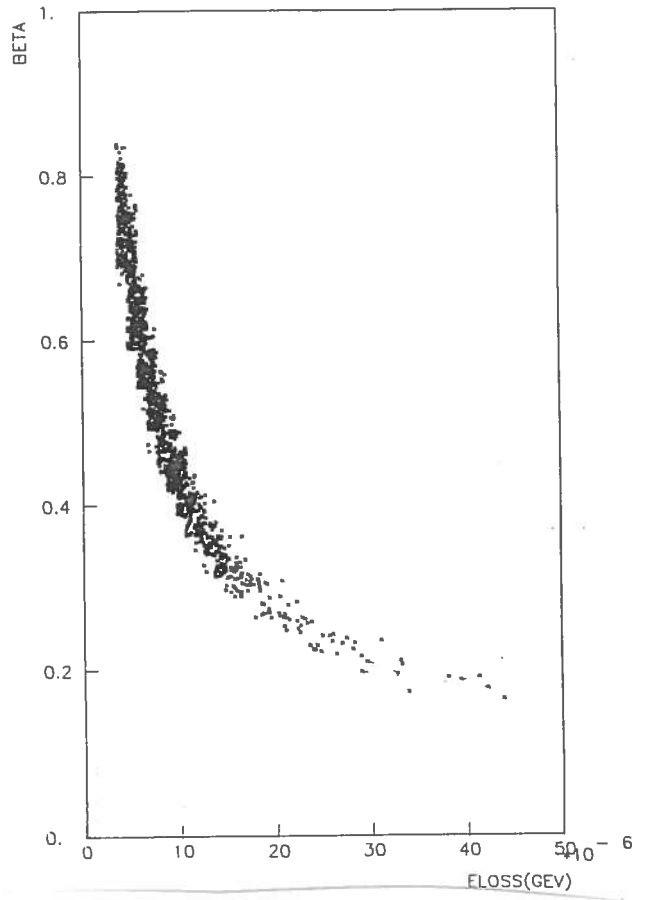

FIG. 10 - β versus energy loss, truncated mean (5 out of 10 Ar gaps).

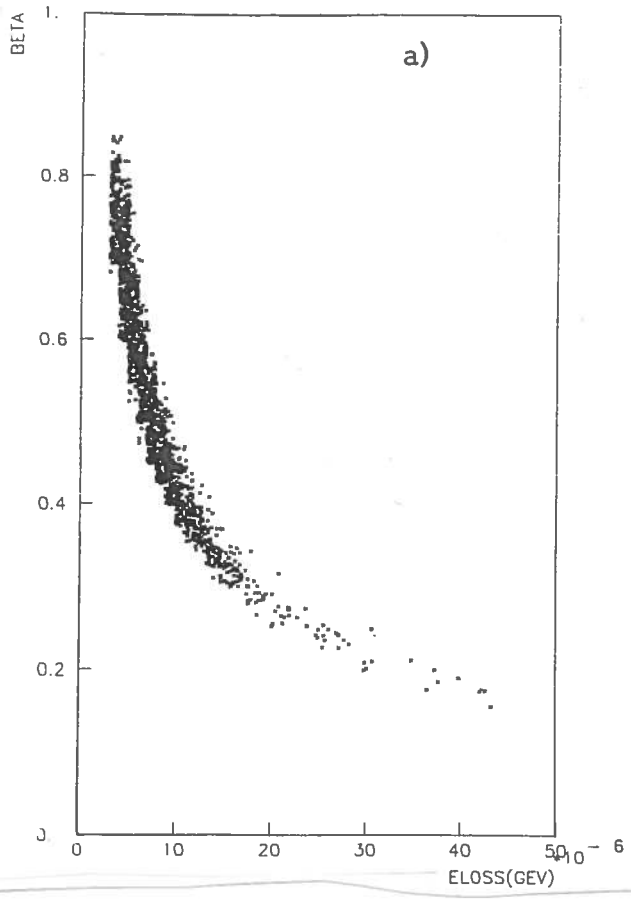

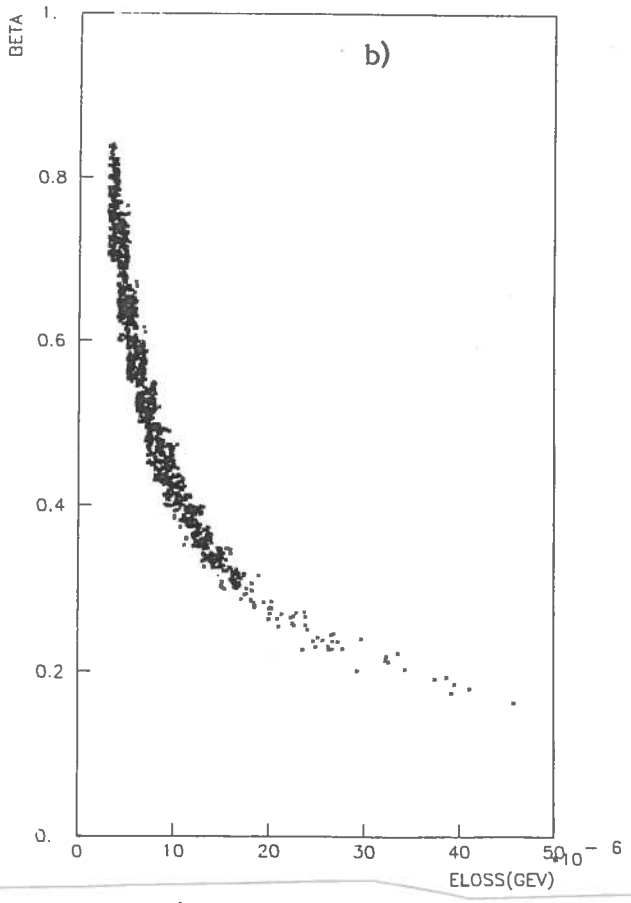

FIG. 11 - β versus energy loss, truncated mean; a) 3 out of 6 gaps; b) 8 out of 15 gaps.

3.2. - Range Measurement

The range of a particle was calculated by integrating its momentum loss over its path in lead. Gaussian fluctuations around the mean range were taken into account according to the formula:

$$R_{RMS} = < R > \sqrt{200\ m(e)/M}\ \ f(\gamma)$$

where M is the mass of the particle, m(e) is the mass of the electron and f is a known empirical function.

Range distributions of the accepted K are plotted in Fig. 12 as a function of β.

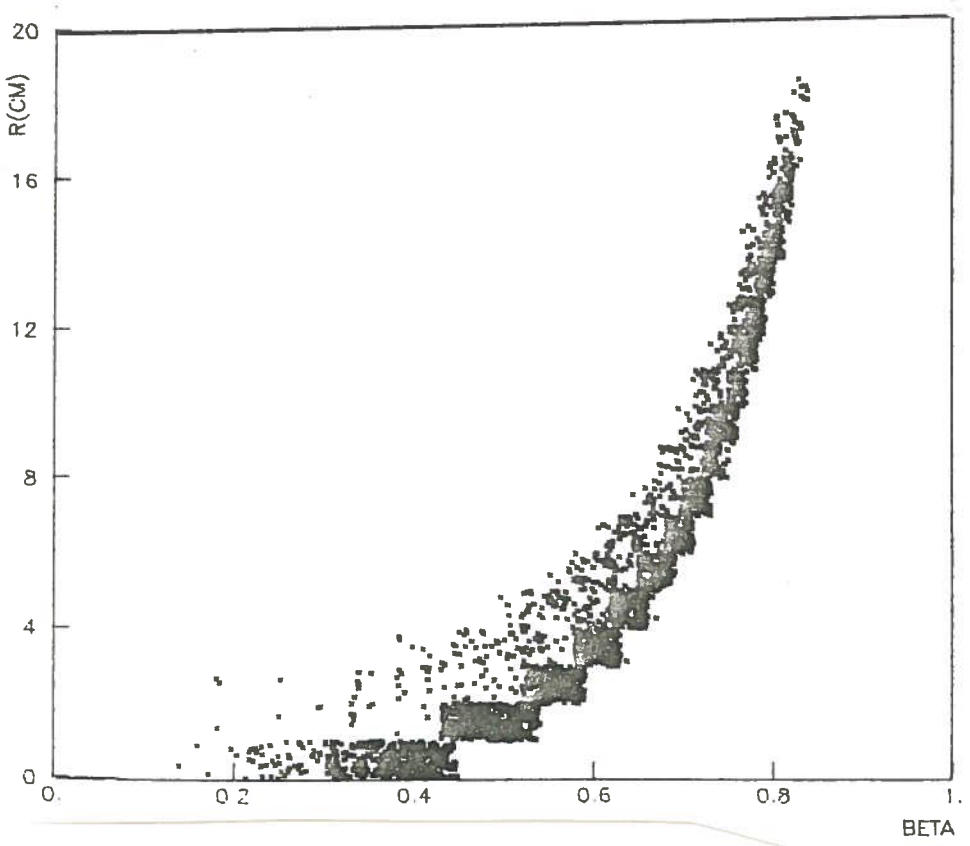

FIG. 12 - Range in Pb for the accepted K momenta, as a function of β.

3.3. - Energy Loss - Range Correlation

As it is shown in Fig. 13, it is possible to define an energy loss-range correlation, by means of which particles are identified.

The following requestes were taken into account in the definition of correlation criteria:

a) the efficiency in K recognition must be high;
b) the rejection of pions and protons must be high;
c) the compactness of the apparatus forbids a high number of range samplings.

To increase the rejection efficiency, an event was rejected if one particle at least does not satisfy the correlation, i.e. it is not recognized as a K. The results of the correlation procedure, applied to a sample of 1998 $\emptyset\ \emptyset$ events in the acceptance, are shown in Table V for different correlations defined as in Table VI-VIII.

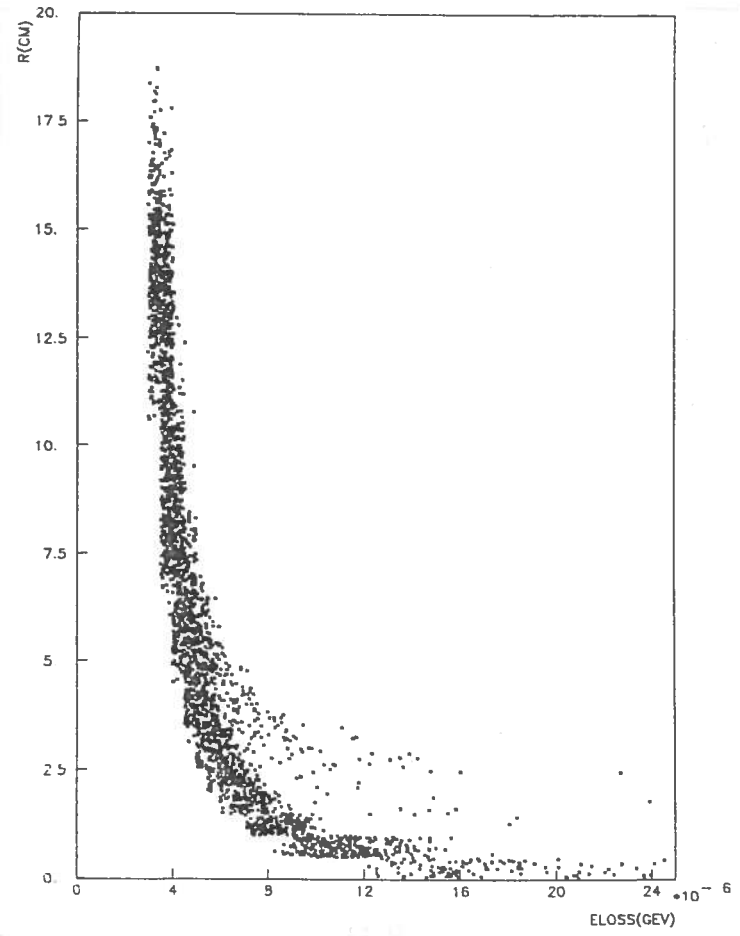

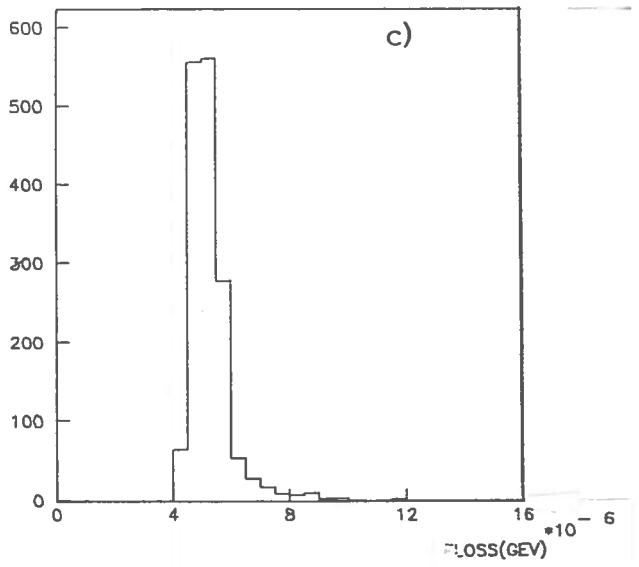

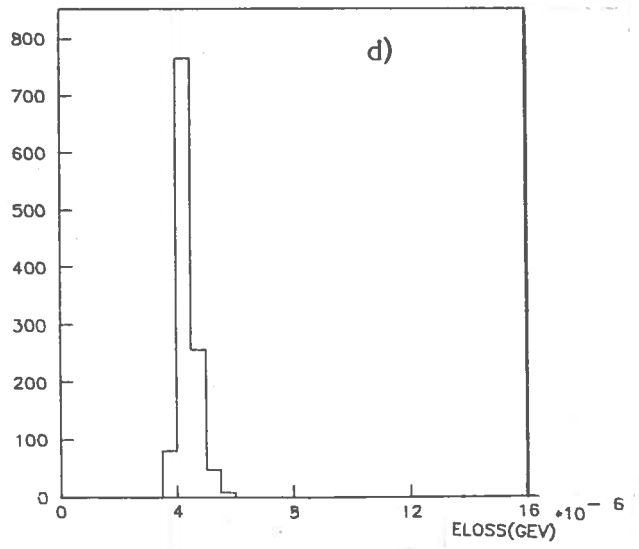

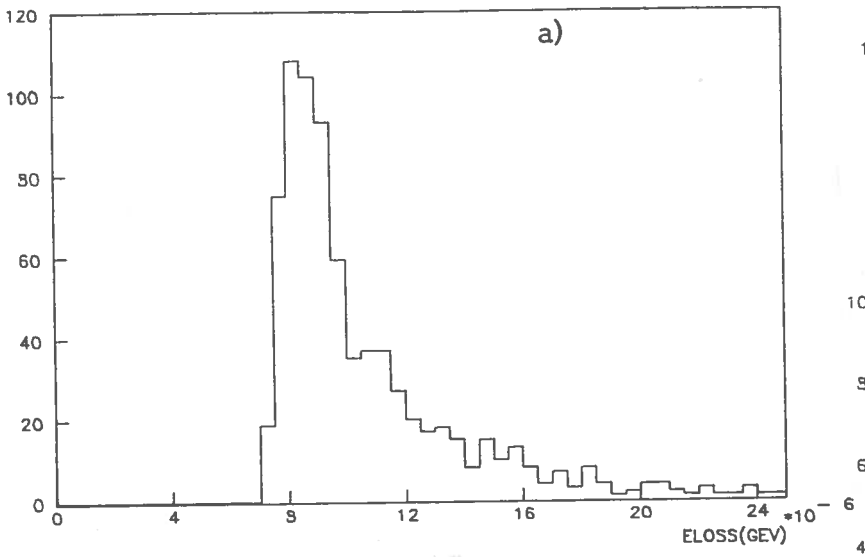

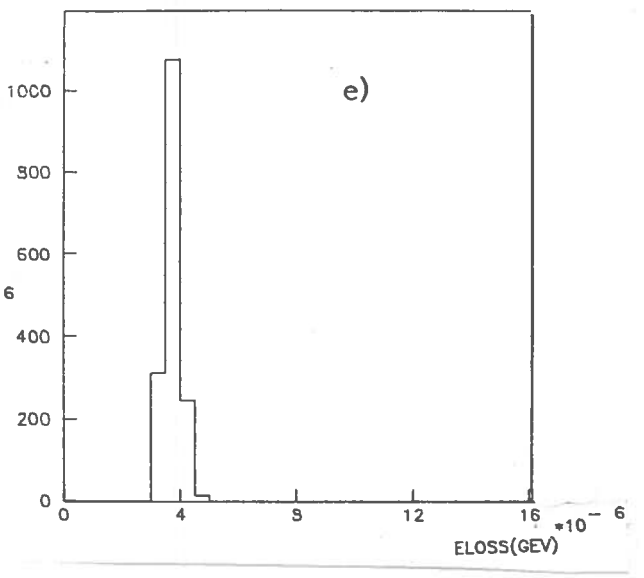

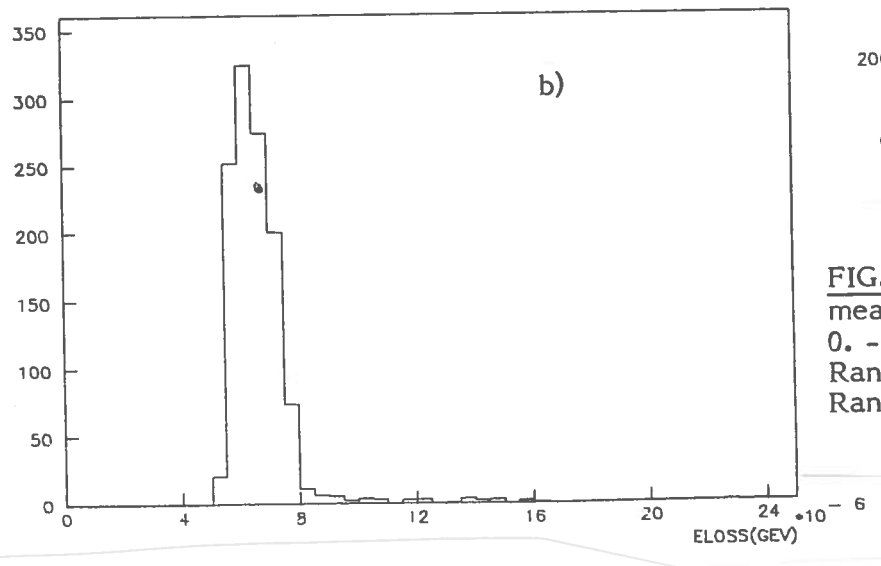

FIG. 13 - Range versus energy loss, truncated mean 5 out of 10, for the accepted K: a) Range 0. - 1.5 cm, energy loss tr. m. distribution; b) Range 1.5. - 3. cm; c) Range 3. - 5.5 cm; d) Range 5.5 - 8.0 cm; e) Range 8.0 - 18.0 cm.

TABLE V - K identification efficiency for different correlations.

Correlation 1	Correlation 2	Correlation 3
a) 98.9	a) 99.7	a) 99.8
b) 96.5	b) 99.1	b) 99.4

TABLE VI - Range-energy loss correlation (1).

Range (cm)	En. loss (keV)
0. - 0.5	13. - 50.
0.5 - 1.	8.5 - 14.
1. - 1.5	7. - 10.5
1.5 - 2.5	5.5 - 10.5
2.5 - 4.	4.5 - 10.
4. - 6.5	4. - 7.5
6.5 - 18.	3. - 5.

TABLE VII - Range-energy loss correlation (2).

Range (cm)	En. loss (keV)
0. - 1.5	7. - 50.
1.5 - 3.	5. - 15.
3. - 5.5	4. - 10.
5.5 - 8.	3.5 - 6.
8. - 18.	3. - 5.

TABLE VIII - Range-energy loss correlation (3).

Range (cm)	En. loss (keV)
0. - 1.5	7. - 50.
1.5 - 3.	5. - 15.
3. - 5.5	4. - 10.
5.5 - 8.	3.5 - 6.

The effect on the recognition efficiency of the choice of the number of analog chamber gaps and of the corresponding fraction of measurements retained is shown in Table IX.

TABLE IX - Recognition efficiency with different NMEAS/NTOT (correlation 1). a) is single track recognition efficiency (%); b) is event recognition efficiency (%).

NMEAS/NTOT	Efficiency	
3/6	a)	98.6
	b)	95.5
5/10	a)	98.9
	b)	96.5
8/15	a)	99.2
	b)	97.3

3.4. - Background Processes

Some background processes were considered to check the capability of discriminating different kinds of particles.

The following processes, whose cross sections are in Table X, were generated with equal number of events in the acceptance shown in Table XI:

$p\bar{p} \rightarrow \pi^+\pi^-\pi^+\pi^-$

$p\bar{p} \rightarrow K^+K^-\pi^+\pi^-$

$p\bar{p} \rightarrow p\bar{p}\,\pi^+\pi^-$

TABLE X - Background total cross sections.

Reaction	Cross section (mb)
$\pi^+\pi^-\pi^+\pi^-$	2.5
$K^+K^-\pi^+\pi^-$	2.
$p\bar{p}\,\pi^+\pi^-$	0.003

TABLE XI - Acceptance for some background processes.

Reaction	Acceptance (%)
$\pi^+\pi^-\pi^+\pi^-$	5.4
$K^+K^-\pi^+\pi^-$	6.5
$p\bar{p}\,\pi^+\pi^-$	1.0

These processes exhibit the range-energy loss features plotted in Fig. 14. The same correlations previously defined to recognize a K were applied to these reactions too; the rejection power against these background events is very high, as it results from Table XII.

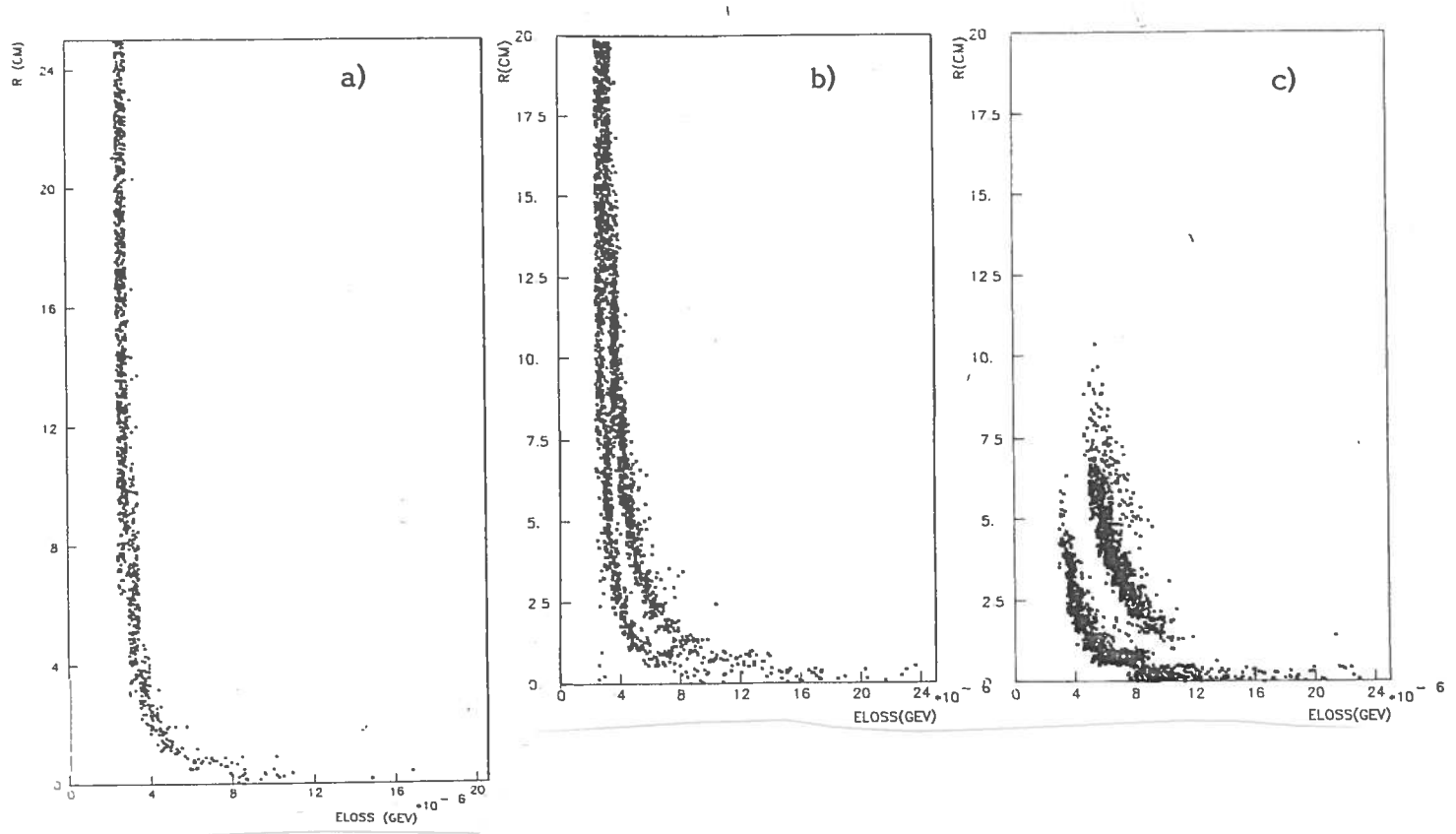

FIG. 14 - Range versus energy loss, tr. m. 5 out of 10, for the background processes, a) $p\bar{p} \rightarrow \pi^+\pi^-\pi^+\pi^-$, b) $p\bar{p} \rightarrow K^+K^-\pi^+\pi^-$, c) $pp \rightarrow pp\ \pi^+\pi^-$.

TABLE XII - Rejection efficiency against background processes for different correlation definitions.

Reaction	Correlation 1	Correlation 2	Correlation 3
$\pi^+\pi^-\pi^+\pi^-$	a) 3.0	a) 5.2	a) 93.3
	b) 100.	b) 100.	b) 19.8
$K^+K^-\pi^+\pi^-$	a) 30.9	a) 33.2	
	b) 99.8	b) 99.8	
$p\bar{p}\pi^+\pi^-$	a) 42.9	a) 56.0	
	b) 98.0	b) 92.2	

A further help in rejecting these background events should come from a kinematical fitting.

The possibility of a pion to be absorbed because of nuclear interactions in lead was considered too: by associating the particle to a path smaller than its range in lead, it could simulate an energy loss-range correlation typical of a K. As a first approximation a constant absorption path in Pb of 18.3 cm was assumed.

The range versus β distribution and the energy loss-range correlation are modified as in Figs. 15-16, to be compared with Fig. 14, for a background process

$$p\bar{p} \longrightarrow \pi^+\pi^-\pi^+\pi^- \qquad (11)$$

However, the rejection efficiency is not affected very much by this effect (Table XIII).

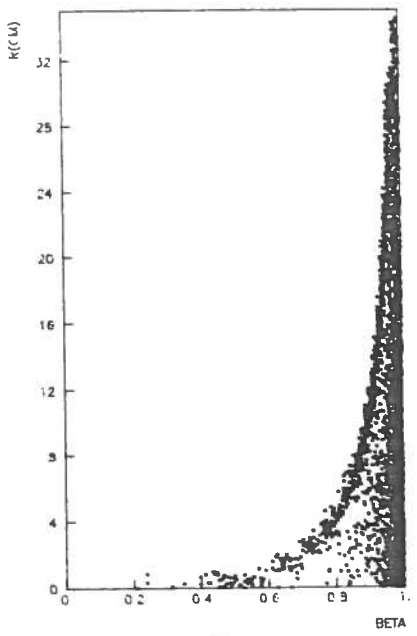

FIG. 15 - Range versus β for the accepted π from $p\bar{p} \longrightarrow 4\pi$, with π absorption in lead.

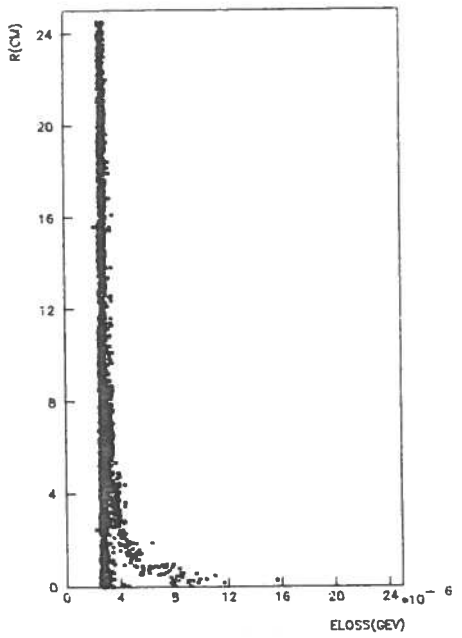

FIG. 16 - Range versus energy loss, tr. m. 5 out of 10, same as Fig. 15.

TABLE XIII - Rejection efficiency including the effect of nuclear interactions in Pb. a) is the efficiency for the single track recognition as a K (%); b) is event rejection efficiency (%).

Reaction	Efficiency	
$\pi^+\pi^-\pi^+\pi^-$	a)	4.4
	b)	100.
$K^+K^-\pi^+\pi^-$	a)	33.2
	b)	99.8
$p\bar{p}\pi^+\pi^-$	a)	54.9
	b)	92.2

3.5. - Particle Identification in other Processes

The method previously described does not provide meaningful information in the case of the processes

$$p\bar{p} \rightarrow \xi \rightarrow K^o_s K^o_s \rightarrow \pi^+\pi^-\pi^+\pi^- \qquad (12)$$

$$p\bar{p} \rightarrow \xi \rightarrow K^+ K^- \qquad (13)$$

since, as it is shown in Fig. 7, the reaction products cover a range of too high β, corresponding to a region near or above the minimum of the energy loss curve and resulting in a large range.

This is in particular true for reaction (13) as it is shown in Fig. 17, while energy loss-range correlation can be of some help in rejecting some background events in the case of reaction (12) (Fig. 18). For instance, with a correlation defined as in Table XIV, the recognition efficiency is 98.9%, while the rejection efficiency of background events

$$p\bar{p} \rightarrow K^+ K^- K^+ K^-$$

is = 99.2%. However, the of the background process

$$p\bar{p} \rightarrow \pi^+\pi^-\pi^+\pi^-$$

satisfy the correlation criteria too and should be rejected by a further kinematical fitting.

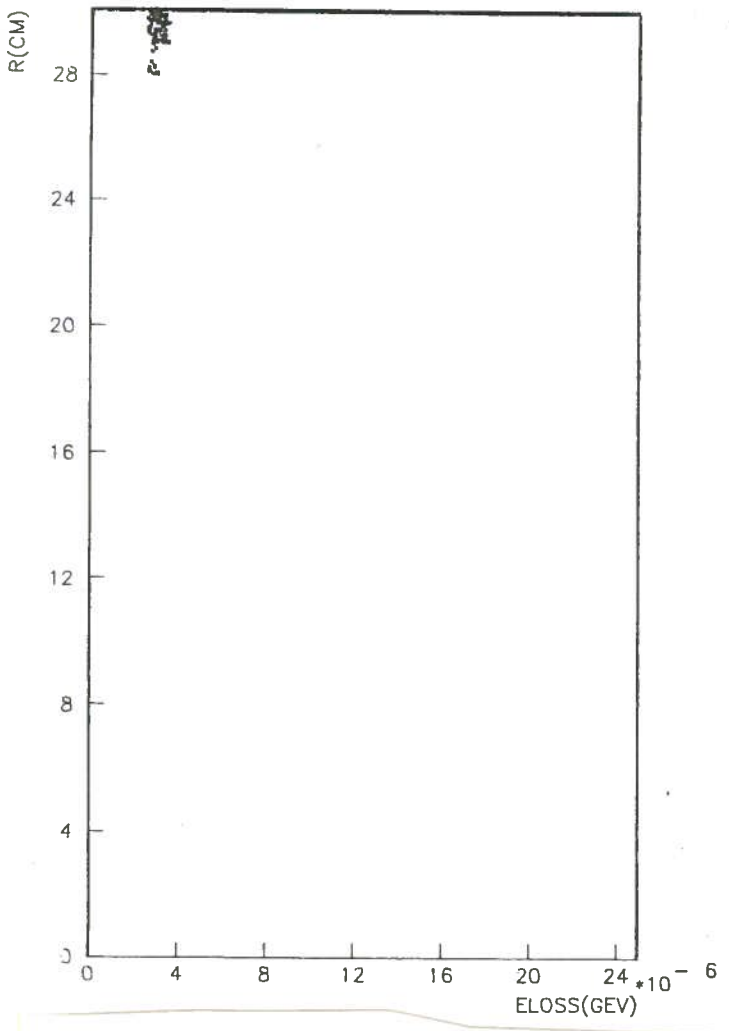

FIG. 17 - Range versus energy loss, tr. m. 5 out of 10, for the accepted K from $\xi \rightarrow K^o_s K^o_s$.

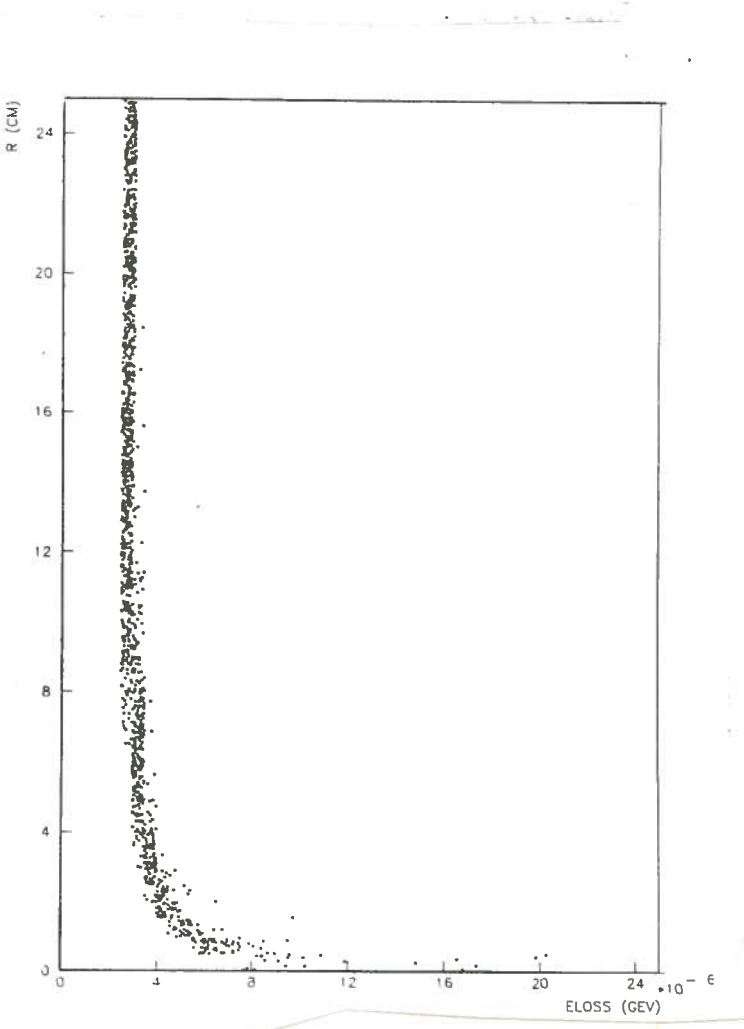

FIG. 18 - Range versus energy loss, tr. m. 5 out of 10, for the accepted π from $\xi \rightarrow K^o_s K^o_s$.

TABLE XIV - Correlation definition for π from $K^o_s K^o_s$.

Correlation 4	
Range (cm)	En. loss (keV)
0. - 1.5	4.5 - 11.
1.5 - 3.	3.5 - 5.5
3. - 5.5	3. - 4.
5.5 - 8.	2.5 - 3.5
8. - 18.	2.5 - 3.5
> 18.	2.5 - 3.

A more complete statistics of the rejection of background processes can be found in Table XV.

In the study of these processes pion absorption because of nuclear interactions in lead was neglected.

TABLE XV - Rejection efficiency of background processes with correlation 4. a) is the efficiency for the single track recognition as a K (%); b) is event rejection efficiency (%).

Reaction	Efficiency	
$K^+K^-K^+K^-$	a)	18.6
	b)	99.2
$K^+K^-\pi^+\pi^-$	a)	65.4
	b)	79.9
$p\bar{p}\pi^+\pi^-$	a)	52.8
	b)	99.6

4. - EXPERIMENTAL APPARATUS

The results of the Montecarlo simulation suggest some features of the experimental apparatus. The longitudinal section of a possible set-up is sketched in Fig. 19, where:

- CH1 is a multiwire proportional chamber;
- AC is an analog chamber;
- CHR1 ... CHR6 are range detectors;
- S1, S2 are trigger counters.

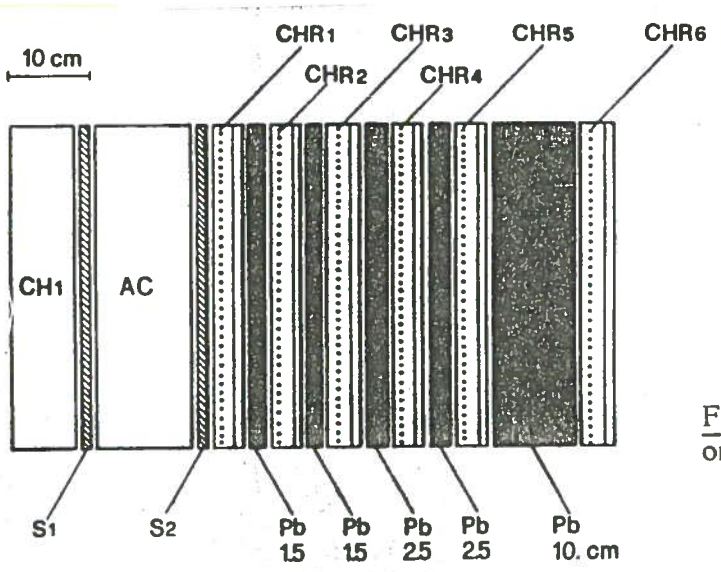

FIG. 19 - Sketch of the longitudinal section for one arm of a possible detector.

In each arm track directions are measured by two digital chambers (CH1, CHR1). The lever arm between the two chambers can be very short; in fact the precision in track reconstruction is limited by multiple scattering in the vacuum chamber mainly. Assuming a 2 mm wire spacing for CH1 and CHR1, the error in vertex reconstruction due to the distance d between these two chambers is smaller than the error due to multiple scattering in the vacuum chamber for $d \gtrsim 9$ cm.

As a possible detector to measure energy loss, analog chambers AC[(1)] were considered. As studied in Chapt. 3., a set of 10 independent measurements may be sufficient to reduce the effect of Landau fluctuations. These chambers can provide a further position measurement.

A sandwich of lead layers and active detectors is used for range sampling. The CHR detectors can be digital chambers, each one with two gaps and a few mm wire spacing. These detectors would allow the reconstruction of different tracks, including those deriving from K decay, thus improving the acceptance.

As discussed in Chapt. 3., five range samplings should be necessary at least.

Trigger counters S1 and S2 are placed immediately after CH1 and before CHR1; a hodoscope structure can be foreseen for S2 at least. A system of anticoincidence counters should cover as much as possible of the free space among the arms.

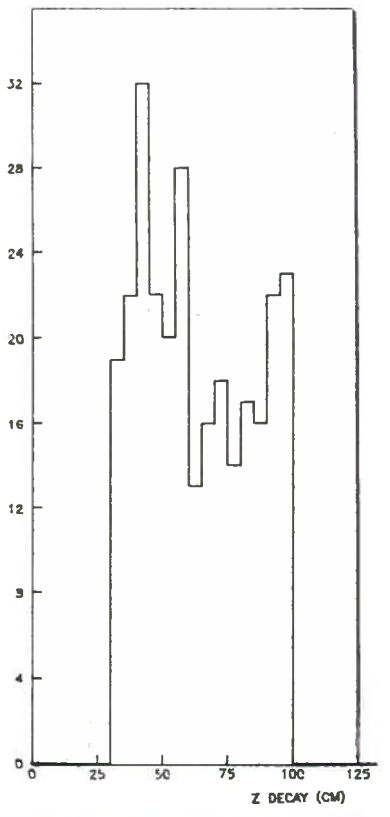

FIG. 20 - Distribution of Z-decay coordinate for K decaying inside the apparatus, with Zmin=30 cm and Zmax=100 cm.

The total length Zmax along the arm axis is about 100 cm; the corresponding acceptance, assuming the standard angular configuration, is:

- 7.7% requesting 3 K at least inside the apparatus;
- 1.3% requesting 4 K inside the apparatus.

In this calculation the effect of energy loss in lead on K lifetime was not taken into account.

The distribution of Z-coordinate of the fourth K decaying in the apparatus is plotted in Fig. 20.

BIBLIOGRAPHY

(1) C. Baglin et al., Spectroscopy at ISR using an antiproton beam and a H_2 gas "Jet target", EP report, to be published.
(2) C. Baglin et al., Letter of intent, CERN/PSSC/84-22, March 1984.
(3) W. Toki, MARK III results from SPEAR, SLAC-Pub-3262, (1983).
(4) V.C. Ermilova et al., Nucl. Instr. & Meth 145, 555 (1977).